Improvements in the Monthly Gravity Field Solutions Through Modeling the Colored Noise in the GRACE Data

Guo, Xiang; Zhao, Qile; Ditmar, Pavel; Sun, Yu; Liu, Jingnan

DOI
10.1029/2018JB015601

Publication date
2018

Document Version
Final published version

Published in
Journal of Geophysical Research: Solid Earth

Citation (APA)
Guo, X., Zhao, Q., Ditmar, P., Sun, Y., & Liu, J. (2018). Improvements in the Monthly Gravity Field Solutions Through Modeling the Colored Noise in the GRACE Data. *Journal of Geophysical Research: Solid Earth*, *123*(8), 7040-7054. https://doi.org/10.1029/2018JB015601

Journal of Geophysical Research: Solid Earth

RESEARCH ARTICLE
10.1029/2018JB015601

Improvements in the Monthly Gravity Field Solutions Through Modeling the Colored Noise in the GRACE Data

Xiang Guo[1], Qile Zhao[1], Pavel Ditmar[2], Yu Sun[3], and Jingnan Liu[1]

[1]GNSS Research Center, Wuhan University, Wuhan, China, [2]Faculty of Civil Engineering and Geosciences, Delft University of Technology, Delft, Netherlands, [3]Key Lab for Data Mining and Information Sharing, Ministry of Education, Fuzhou University, Fujian, China

Key Points:
- Colored noise in GRACE data is accounted for in the dynamic approach by applying the frequency-dependent data weighting (FDDW) scheme
- Application of the FDDW scheme substantially reduces the noise level in the obtained GRACE monthly gravity field solutions
- The FDDW scheme significantly improves consistency between GRACE and the state-of-the-art hydrology model WaterGAP over the Mississippi and Congo river basins

Correspondence to:
Q. Zhao,
zhaoql@whu.edu.cn

Citation:
Guo, X., Zhao, Q., Ditmar, P., Sun, Y., & Liu, J. (2018). Improvements in the monthly gravity field solutions through modeling the colored noise in the GRACE data. *Journal of Geophysical Research: Solid Earth*, *123*. https://doi.org/10.1029/2018JB015601

Received 6 FEB 2018
Accepted 19 JUL 2018
Accepted article online 27 JUL 2018

Abstract The Gravity Recovery And Climate Experiment (GRACE) mission has achieved a quantum leap in knowledge of the Earth's gravity field. However, current gravity field solutions still cannot reach the prelaunch baseline accuracy. One of the reasons for that is the presence of colored noise in GRACE data, which is typically ignored in the classical dynamic approach to gravity field modeling. In this research, we propose to account for colored noise in the classical dynamic approach by applying the frequency-dependent data weighting (FDDW) scheme, so that enhanced estimates of gravity field solutions are produced. The monthly solutions are compared with those produced using the standard least squares adjustment without a data weighting scheme. The comparison is performed in both spectral and spatial domains, showing the positive effect of the FDDW scheme in all considered cases. For instance, the cumulative geoid height errors up to degree 96 are reduced by 18%. In the spatial domain, the FDDW scheme lowers noise level in mass changes over the oceans, Mississippi river basin, and Greenland by 20, 38, and 23%, respectively, when compared to the without a data weighting scheme. In addition, the consistency of mass changes over the Mississippi and Congo river basins with those inferred from the state-of-the-art hydrology model WaterGAP is substantially improved when the FDDW scheme is applied. These results indicate that modeling colored noise in the GRACE data allows to significantly improve the recovered monthly solutions. This finding is likely applicable also to the GRACE Follow-On mission.

1. Introduction

The Gravity Recovery And Climate Experiment (GRACE) satellite mission (Tapley et al., 2004) has provided a lot of information about temporal variations of the Earth's gravity field since 2002. The monthly gravity field solutions, denoted as level-2 products, have been computed using the classical dynamic approach by the official GRACE processing centers: Center for Space Research (CSR; Bettadpur, 2012), Deutsches GeoForschungsZentrum (Dahle et al., 2012), and the Jet Propulsion Laboratory (Watkins & Yuan, 2014). Although accuracy of the gravity field solutions has been significantly improved during the past decade, there still remains a large offset between their error level and the prelaunch baseline accuracy (Kim, 2000).

To compute the monthly gravity field solutions, one must convert the GRACE Level-1b K-Band Range observations into residual data by subtracting their a priori counterparts. The latter are based on a set of background force models, which includes models to describe ocean tides (Chen et al., 2009; Ray & Luthcke, 2006; Seo et al., 2008; Visser et al., 2010), as well as nontidal variations in the atmosphere and ocean (the so-called Atmosphere and Ocean De-aliasing product (Dobslaw et al., 2016)). However, background force models suffer from inaccuracies, which propagate into GRACE data as correlated noise (McCullough & Bettadpur, 2016). Furthermore, GRACE data processing relies upon observations of various onboard instruments, including the accelerometers and star cameras, which are not perfect as well (Inácio et al., 2015; Klinger & Mayer-Gürr, 2016). Finally, the K-Band Range observations are typically converted either into K-Band Range-Rate (KRR) data or into intersatellite accelerations by means of differentiation in time, which amplifies high-frequency noise (Wu et al., 2006). As a result, noise in GRACE data may be strongly dependent on frequency (Ditmar et al., 2012).

To account for noise correlations in satellite instrument data, a concept of frequency-dependent data weighting (FDDW) was developed. This concept stems from the fast collocation technique (Bottoni & Riccardo, 1993). It is based on the assumption of stationary noise in the measurements, so that the noise

Table 1
Data and Models Used for Gravity Field Recovery

Background force models	Description
Mean gravity field model	EIGEN-6C4 (Förste et al., 2014; 180×180)
Solid Earth and pole tides	IERS Conventions 2010 (Petit & Luzum, 2010)
Ocean tides	EOT11a (Rieser et al., 2012; 120×120)
Ocean pole tides	Desai (Desai, 2002; 30×30)
Atmosphere and ocean de-aliasing	AOD1B RL05 (Flechtner et al., 2015)
Third-body perturbations	DE421 (Folkner et al., 2009)
General relativistic effects	IERS Conventions 2010 (Petit & Luzum, 2010)
Reference frames	
Conventional inertial reference frame	IERS Conventions 2010 (Petit & Luzum, 2010)
Precession/nutation	IAU 2006/2000A (Petit & Luzum, 2010)
Earth orientation parameters	IERS EOP 08 C04
Input data	
Reduced-dynamic orbit	Level 1B RL02, 5-min sampling
K-band range-rate measurements	Level 1B RL02, 5-s sampling
GRACE attitudes	Level 1B RL02, 5-s sampling
Nongravitational accelerations	Level 1B RL02, 5-s sampling
Estimated parameters	
Initial state vector	Position and velocity per satellite and per arc
Accelerometer bias	Piecewise constant
Accelerometer scale	One per month per component
Spherical harmonic coefficients	Complete to degree and order 96

covariance matrix has the Toeplitz structure. Such a matrix can be approximated by a circulant one. According to the convolution theorem, the time-consuming cyclic convolution in the time domain corresponds to an element-wise multiplication in the frequency domain, which allows FDDW to be efficiently applied to large data sets. The FDDW concept has been discussed in detail and further extended to account for nonstationary data noise in Ditmar et al. (2007). Among others, those authors successfully used that concept to estimate the static Earth's gravity field from the CHAMP satellite accelerations derived from kinematic orbits (Ditmar et al., 2006). This concept was adopted later to produce the Delft Mass Transport model from GRACE intersatellite accelerations (Farahani et al., 2014; Liu et al., 2010).

An alternative approach to handle correlated noise is to construct a fully populated observation covariance matrix. Recent researches showed that modeling the correlated errors in this way can obviate the need for estimating kinematic empirical parameters during the solution process and drastically improve formal errors of the GRACE monthly gravity field solutions (McCullough & Bettadpur, 2016). However, introducing such a covariance matrix inevitably increases the numerical complexity, especially in case of large data sets (such as those used in gravity field modeling).

In this study, we use for the first time the FDDW concept to deal with colored noise in KRR observations in the context of the dynamic approach to the computation of GRACE monthly gravity field solutions. In addition, we produce monthly solutions using the standard least squares adjustment without data weighting (WODW). Then, we analyze the impact of different data weighting methods by comparing the monthly solutions in both the spectral and spatial domains.

This paper is organized as follows: section 2 presents details of data and methods adopted for producing the monthly solutions. Results are shown in section 3. Finally, section 4 is left for conclusions.

2. Data and Methods

2.1. Input Data and Background Models

Our study is based on the Position And Navigation Data Analyst (PANDA) software. This software was developed at the GNSS Research Center of Wuhan University and has been widely used in precise orbit determination for both GNSS satellites and low Earth orbiters (Liu & Ge, 2003; Shi et al., 2008). In recent years, the dynamic approach to gravity field modeling has been implemented in PANDA and successfully applied to produce GRACE monthly gravity field solutions (Guo & Zhao, 2018; Zhao et al., 2011). The strategy adopted is described in Table 1. Relatively short (6-hr) arcs are used to reduce the resonance effects caused by inaccuracies in initial state vectors and background models (Colombo, 1984) on the one hand and to enable more efficient concurrent processing on the other hand. Both the KRR measurements and the Reduced-Dynamic Orbits (RDO) are used as observations in our data processing. Although a RDO suffers from a bias toward the prior gravity field information, the resulting bias in the gravity field solutions has been proved to be minor, since the weight of those data is small when compared to that of the KRR measurements (Chen et al., 2014).

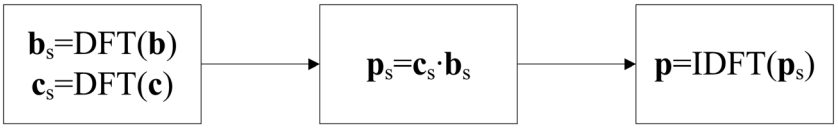

Figure 1. Flow chart of the computation **p** = **Cb** with the FDDW scheme.

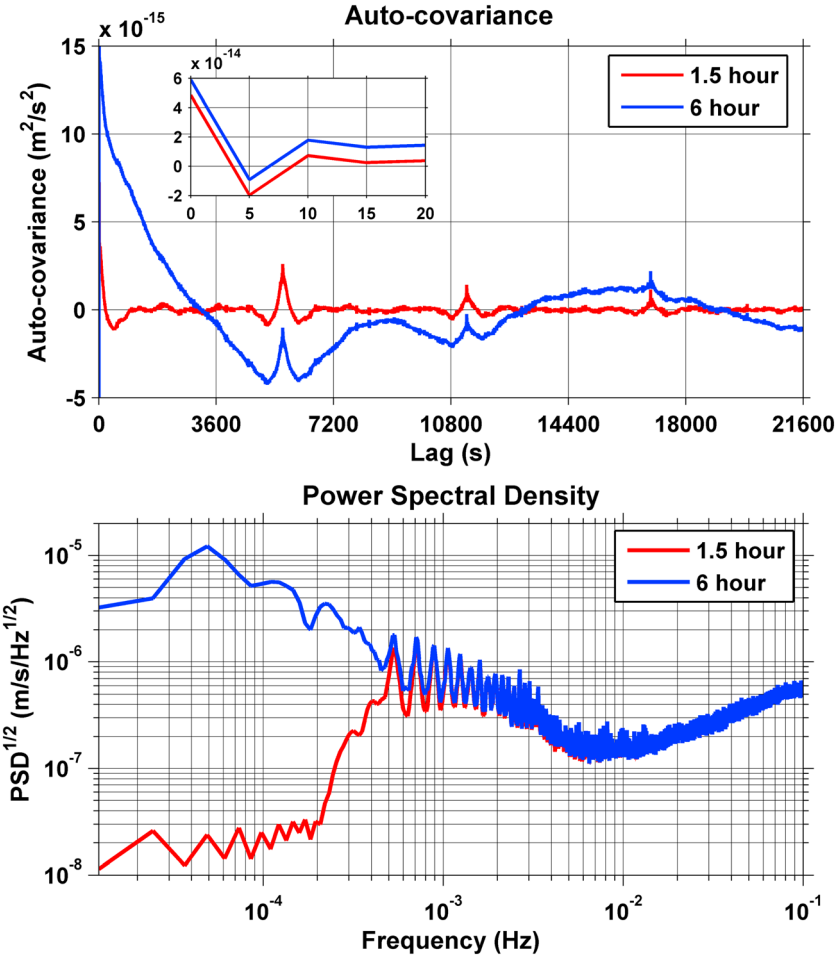

Figure 2. (top) Auto-covariance and (bottom) $PSD^{1/2}$ of the postfit KRR residuals, where the accelerometer bias parameters are estimated per 6-hr (blue line) and 1.5-hr (red line) interval. The month under consideration is April 2006.

2.2. Data Weighting Scheme

With the weighted least squares approach, the unknown parameter vector **X** can be obtained as

$$\mathbf{X} = \left(\mathbf{A}_k^T\mathbf{C}_k^{-1}\mathbf{A}_k + \mathbf{A}_o^T\mathbf{C}_o^{-1}\mathbf{A}_o\right)^{-1}\left(\mathbf{A}_k^T\mathbf{C}_k^{-1}\mathbf{d}_k + \mathbf{A}_o^T\mathbf{C}_o^{-1}\mathbf{d}_o\right) \quad (1)$$

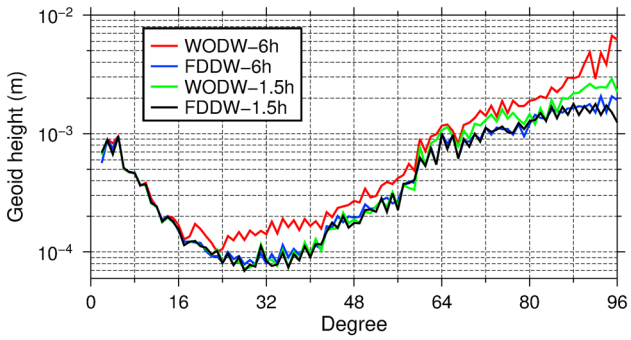

Figure 3. Geoid height differences per degree with respect to EIGEN-6C4 for the solutions produced with different weighting schemes and estimation intervals of accelerometer biases.

where **A** is a design matrix, **d** is a residual observation vector (observed minus computed), and **C** is a noise covariance matrix (its inverse is used to weigh the observations); the subscript "k" stands for the KRR observations and "o" for the orbit observations. Usually, $\sum\mathbf{A}^T\mathbf{C}^{-1}\mathbf{A}$ is denoted as the normal matrix, and $\sum\mathbf{A}^T\mathbf{C}^{-1}\mathbf{d}$ as the right-hand side vector.

Here we consider the application of two data weighting schemes (WODW and FDDW) to the KRR observations.

In the case of the commonly used WODW scheme, the weight of the KRR observations is set based on a priori information about their precision, 0.2 μm/s. Thus, the covariance matrix $\mathbf{C_k}$ is a unit one scaled by a constant factor. In this case, the associated normal matrix and the right-hand side vector can be easily computed observation-by-observation.

As regards the FDDW scheme, in view of the assumption of stationary noise in the KRR measurements, the noise covariance matrix $\mathbf{C_k}$ is

Table 2
Cumulative Geoid Height Differences (mm) With Respect to EIGEN-6C4 for Solutions Produced With Different Weighting Schemes and Estimation Intervals of Accelerometer Biases

	6 hr			1.5 hr			$\frac{1.5\text{ hr}-6\text{ hr}}{6\text{ hr}}$	
Degree	WODW	FDDW	$\frac{\text{FDDW}-\text{WODW}}{\text{WODW}}$	WODW	FDDW	$\frac{\text{FDDW}-\text{WODW}}{\text{WODW}}$	WODW	FDDW
60	2.75	2.36	−14%	2.38	2.36	−1%	−13%	−0%
96	16.47	8.22	−50%	10.34	7.86	−24%	−37%	−4%

Toeplitz; that is, its contents are fully defined by the noise auto-covariance vector **c**. In this research, the noise auto-covariance is estimated from the postfit residuals of the KRR observations as proposed by Ditmar et al. (2007). Let us denote the covariance between epochs i and $i \pm j$ as c_j, an element of the auto-covariance vector with index j. It can be estimated as follows:

$$c_j = \frac{1}{N_j}\sum_i v_i v_{i\pm j} \quad (0 \le j \le n) \tag{2}$$

where v_i and $v_{i \pm j}$ are the postfit residuals at two epochs separated by lag j, n is the maximum lag for which the auto-covariance is estimated, and N_j is the number of pairs of elements used in the estimation of c_j. It should be noted that both elements of each pair should have indices in the interval (1, N), where N is the total number of residuals. In practice, it is advisable to choose $n < N/10$ (Klees et al., 2003).

Once the auto-covariance vector **c** is obtained, it is extended to form a periodic one, so that the covariance matrix $\mathbf{C_k}$ becomes circulant:

$$\mathbf{C}_k = \begin{bmatrix} c_0 & c_1 & \cdots & c_n & \mathbf{0} & c_n & \cdots & c_2 & c_1 \\ c_1 & c_0 & c_1 & \cdots & c_n & \mathbf{0} & c_n & \cdots & c_2 \\ \vdots & \ddots & \ddots & \ddots & \ddots & \ddots & \ddots & \ddots & \vdots \\ c_n & \cdots & c_1 & c_0 & c_1 & \cdots & c_n & \mathbf{0} & \\ \vdots & \ddots & \cdots & \ddots & \ddots & \ddots & \cdots & \ddots & \vdots \\ & \mathbf{0} & c_n & \cdots & c_1 & c_0 & c_1 & \cdots & c_n \\ \vdots & \ddots & \ddots & \ddots & \cdots & \ddots & \ddots & \cdots & \vdots \\ c_2 & \cdots & c_n & \mathbf{0} & c_n & \cdots & c_1 & c_0 & c_1 \\ c_1 & c_2 & \cdots & c_n & \mathbf{0} & c_n & \cdots & c_1 & c_0 \end{bmatrix} \tag{3}$$

Multiplication of the matrix $\mathbf{C_k}^{-1}$ to a data vector or to a column of the design matrix is implemented by means of the preconditioned conjugate-gradient method. This is an iterative method, which reduces to a matrix-to-vector multiplication of the kind $\mathbf{p} = \mathbf{C_k b}$ at each iteration. The dimension of vector **b** is forced to be consistent with that of matrix $\mathbf{C_k}$ (the added elements are set equal to zero). The matrix-to-vector operation $\mathbf{p} = \mathbf{C_k b}$ is implemented based on the Fourier transform as shown in Figure 1, where DFT denotes the discrete Fourier transform, IDFT denotes its inverse, and the subscript "s" indicates the spectrum. To account for edge effects and data gaps, an appropriate mask is applied to the resulting vector **p**. To minimize the number of preconditioned conjugate-gradient iterations, the circulant approximation of $\mathbf{C_k}$ is also used as the preconditioner. At this point, we benefit from the fact that the inverse of the circulant matrix $\mathbf{C_k}$ is also a circulant one, which can be readily obtained by computing IDFT ($\mathbf{c_s}^{-1}$), where $\mathbf{c_s}^{-1}$ is the result of inverting the spectrum $\mathbf{c_s}$ element by element. It has been shown that FDDW can be applied efficiently and accurately using this scheme (Ditmar et al., 2007).

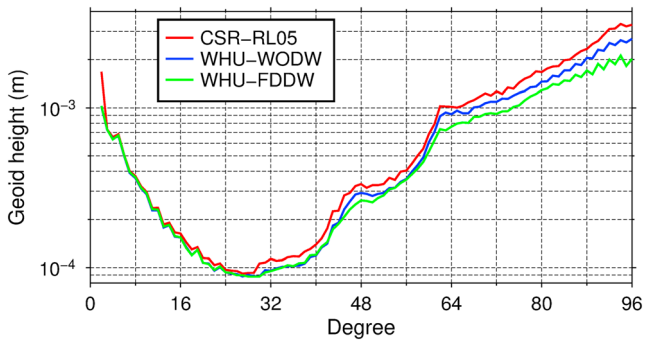

Figure 4. Geoid height differences per degree with respect to GOCO05c for different gravity field solutions (RMS values for 2005–2010).

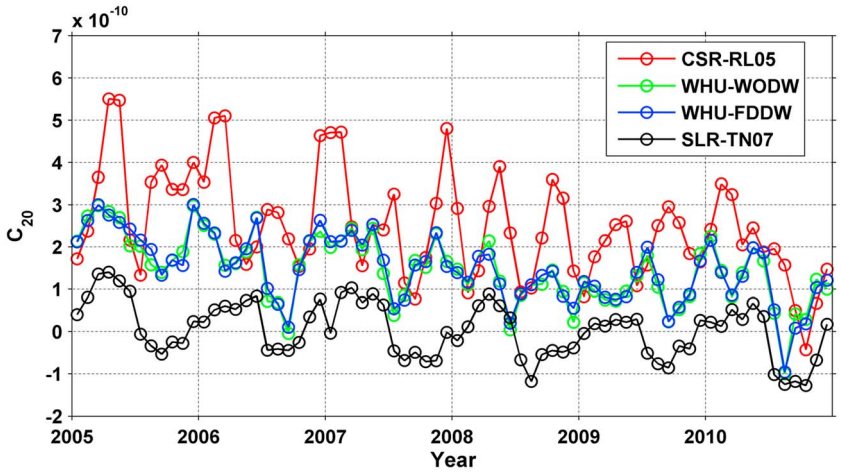

Figure 5. C_{20} time series from different solutions.

As regards the RDO observations, their covariance matrix $\mathbf{C_o}$ is in all cases a unit one scaled by the noise variance σ_o^2, which is assumed to be constant. We set σ_o to be 2 cm in each dimension, which is based on the a priori precision of the GRACE RDOs (Jäggi et al., 2007; Kang et al., 2006).

We believe that the adopted accuracies of KRR and RDO observations are fully justified. They are consistent with those assumed by other groups (Chen et al., 2015; Meyer et al., 2016) and promise the best monthly solutions when applying either data weighting scheme to KRR data.

In principle, the FDDW scheme is applicable also to the RDO observations. However, our test experiments show that the improvements in the gravity solutions are insignificant when one inverts them together with the KRR observations. This is not strange, because the quality of combined KRR/GPS gravity solutions is largely dictated by the KRR observations due to their extremely high precision. Therefore, we decide to adopt a uniform weight for RDOs in all cases during our solution process.

3. Results

Two sets of GRACE monthly gravity field solutions for the time period from January 2005 to December 2010 are produced using the two data weighting schemes. In this section, we will analyze the monthly solutions in both spectral and spatial domains.

3.1. Analysis in the Spectral Domain

As shown in Table 1, the accelerometer biases are estimated as piecewise constant parameters. Here we consider two estimation intervals for the biases: 1.5 and 6 hr. We did not try shorter intervals to avoid a risk of an overparameterization and a signal absorption. Figure 2 displays the auto-covariance and square root of power spectral density of the KRR postfit residuals with different estimation intervals when the FDDW scheme is applied, for a typical month of April 2006. The plots obtained with the WODW scheme are similar and, therefore, not shown here. Please note that scale of the *y* axis in the auto-covariance plot is limited to -5×10^{-15} to 15×10^{-15} m^2/s^2 for a better view. In fact, the maximum and minimum values are obtained at zero and 5-s lags in both cases as shown in the inset plot. It can be seen that both auto-covariance series decrease with time in the beginning and then converge to near zero. A comparison of these two data sets reveals that the 6-hr interval exhibits larger auto-covariances in general, which reflects larger errors in the post-fit residuals. In addition, the 6-hr interval also shows a longer convergence time (about 9,000 s), that is, a larger correlation length, when compared to the 1.5-hr interval (about 900 s). These results indicate that the accelerometer bias parameters estimated per 1.5-hr interval can effectively absorb model errors and reduce their correlation length. We also note that peaks appear at lags near multiples of the orbit revolution period (5,640 s

Table 3
Statistics of the Differences Between C_{20} Coefficients From Different GRACE-Based Solutions and Those From SLR TN07

	Mean (10^{-10})	SD (10^{-10})	RMS (10^{-10})	Correlation coefficients
CSR-RL05	2.48	1.15	2.73	0.427
WHU-WODW	1.42	0.60	1.54	0.676
WHU-FDDW	1.45	0.59	1.56	0.686

Table 4
Cumulative Geoid Height Differences (mm) With Respect to GOCO05c Up to Degree 60 and 96 for Different Gravity Field Solutions (RMS Values in 2005–2010)

Degree	CSR-RL05	WHU-WODW	WHU-FDDW	FDDW−CSR / CSR	FDDW−WODW / WODW
60	2.88	2.39	2.35	−18%	−2%
96	12.08	10.13	8.35	−31%	−18%

in April 2006) and decrease with the increasing lag time in both auto-covariance series. These peaks may be caused by satellite instrument data errors which are dependent on satellite positions, that is, those from the onboard star cameras (Inácio et al., 2015). It should be noted that these peaks are at least 1 order of magnitude smaller than the variances (i.e., the zero lagged auto-covariance) of the respective time series.

As regards the power spectral densities, it can be seen that there exist large low-frequency errors when the 6-hr estimation interval is used. Remember that the power spectrum is the Fourier transform of the auto-covariance. These errors in fact reflect larger auto-covariances and likely result from dynamic orbit errors in this case (Ditmar et al., 2012). On the other hand, these errors are remarkably reduced in the case of the 1.5-hr interval, especially below the 1-cycle-per-revolution frequency. Again, this indicates that the accelerometer biases estimated per 1.5-hr interval can effectively absorb model errors and compensate the orbit deficiencies. Furthermore, large variations of the power spectral densities in both cases support the necessity of the FDDW scheme for an enhanced estimation of gravity field.

In total, four gravity field solutions complete to degree and order 96 for April 2006 are produced using the two data weighting schemes and two estimation intervals of accelerometer biases. Figure 3 shows their differences with respect to EIGEN-6C4 in terms of geoid heights per degree. Note that the differences are actually the coefficient corrections here since EIGEN-6C4 is also used as the background model. Table 2 further lists the cumulative geoid height differences up to degree 60 and 96. From Figure 3 and Table 2, we can see that (1) the FDDW scheme improves the gravity field solution for both bias estimation intervals, (2) the high degrees benefit more from the FDDW scheme than the low ones for both bias estimation intervals, and (3) application of the FDDW scheme significantly reduces the differences between the solutions obtained with different bias estimation intervals. These results demonstrate that the FDDW scheme is rather effective to deal with colored noise in observations and is able to improve the quality of gravity field solutions significantly. Furthermore, these results also show that the 1.5-hr bias estimation interval always yield better solutions than the 6-hr ones (Table 2). We decided, therefore, to use 1.5-hr intervals in the further computations. Note that we did not present the results obtained with intervals between 6 and 1.5 hr to make the discussion

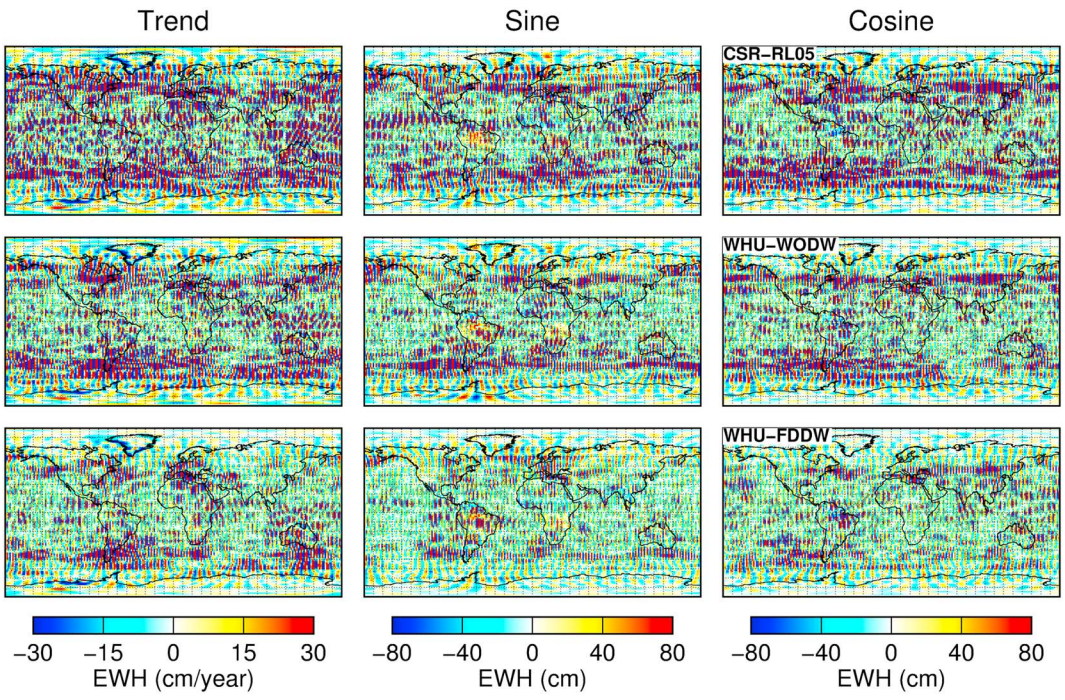

Figure 6. Trends and periodic annual signals in mass changes in terms of equivalent water heights, inferred from unfiltered solutions. The top, middle, and bottom rows display the results based on the CSR-RL05, WHU-WODW, and WHU-FDDW solutions, respectively.

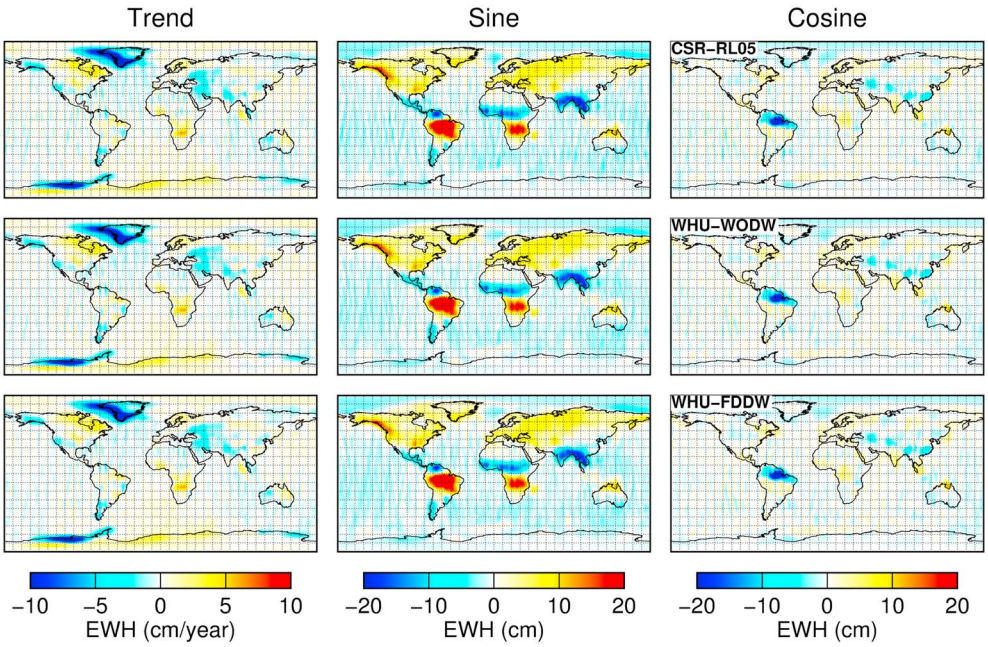

Figure 7. Same as in Figure 6 but for the case of G300 filtered solutions.

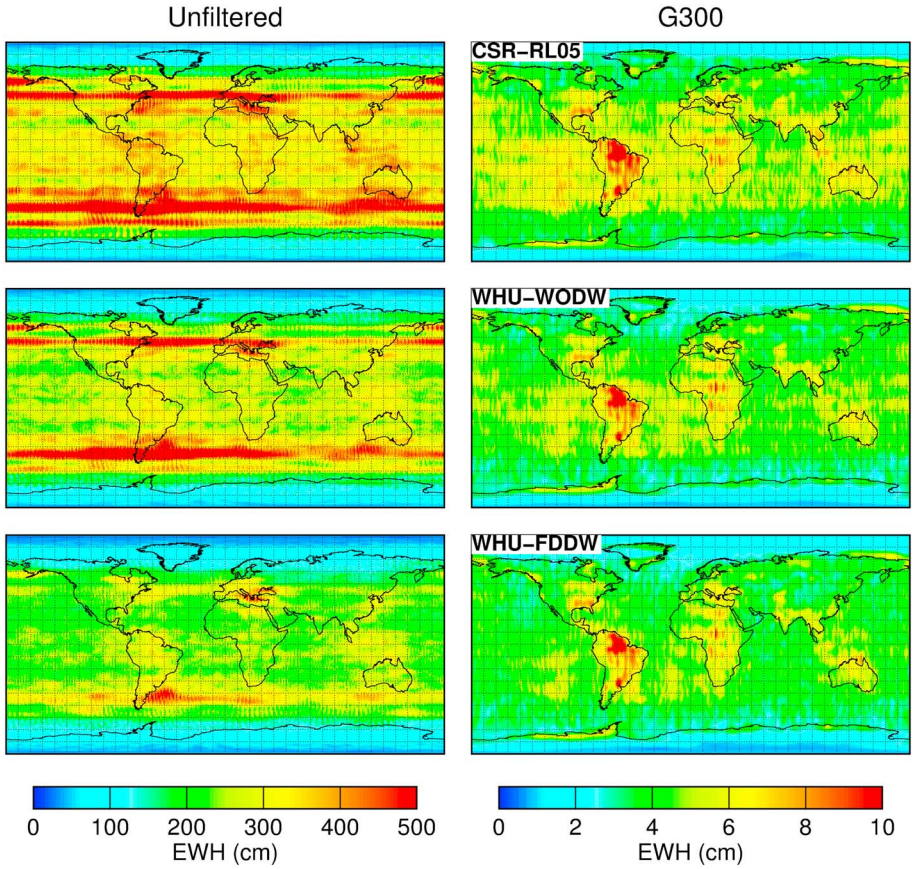

Figure 8. Same as in Figure 6 but for the RMS residuals based on both unfiltered and G300 filtered solutions.

Table 5
Weighted Mean of the RMS Residual Mass Changes (cm) Over Oceans and the Sahara Desert Inferred From Different Solutions (the Gridded RMS Residuals Are Weighted by the Cosine of Latitude)

		CSR-RL05	WHU-WODW	WHU-FDDW	FDDW−CSR / CSR	FDDW−WODW / WODW
Ocean area	Unfiltered	341	291	233	−32%	−20%
	G150	79	68	56	−29%	−18%
	G300	4.9	4.3	4.0	−18%	−7%
Sahara desert	Unfiltered	309	274	251	−19%	−8%
	G150	83	76	72	−13%	−5%
	G300	5.9	5.6	5.4	−8%	−4%

more concise. In fact, we think that the results can be easily deduced from the above comparisons. In principle, a shorter estimation interval means more signal and noise absorption by the bias parameters and thus smaller gravity field corrections.

Hereafter, we compare our solutions with the official CSR-RL05 solutions. We denote our gravity field solutions produced with the FDDW scheme as "WHU-FDDW" and the ones based on the WODW scheme as "WHU-WODW." To make the comparison of the WHU and CSR solutions more objective, an alternative state-of-art static gravity field model GOCO05c (Pail et al., 2016) is used, which is different from the background models exploited in the computation of the WHU and CSR solutions. We subtract the GOCO05c model from all the monthly solutions in the considered time interval (2005–2010). After that, we calculate the RMS (root mean square) from each spherical harmonic coefficient time series. Figure 4 displays the results in terms of geoid heights per degree. One can see that the geoid height differences per degree in the case of the WHU-FDDW solutions are clearly the smallest beyond degree 60, where noise dominates. In addition, large discrepancies between the WHU and CSR solutions can be observed at degree 2. This is mainly caused by large differences in the C_{20} term, to which GRACE is less sensitive due to the polar orbits (Cheng & Ries, 2017). Figure 5 displays the C_{20} time series from different GRACE solutions and SLR TN07 (Cheng et al., 2013), where the mean value (−0.4841694723127E − 03) taken from SLR TN07 has been subtracted from all solutions. It can be observed that clear offsets exist between the GRACE solutions and SLR TN07. But the offsets in the case of the WHU solutions are noticeably smaller than that of CSR-RL05. The mean offsets, standard deviations (SDs), RMSs, and correlation coefficients with respect to SLR TN07 are also computed and listed in Table 3. It can be seen that the WHU solutions agree much better with SLR TN07 than CSR-RL05 does as evidenced by smaller RMSs and larger correlation coefficients for the WHU solutions. On the other hand, the differences of C_{20} between the two WHU solutions are shown to be insignificant, which implies that impact of the weighting scheme on C_{20} estimates is minor.

Table 4 further lists the cumulative geoid height differences with respect to GOCO05c up to degree 60 and 96 for different solutions. In the case of the WHU-FDDW solutions, the cumulative geoid height differences up to degree 96 are reduced by 18 and 31%, respectively, when compared to the WHU-WODW and CSR-RL05 solutions. Therefore, the WHU-FDDW solution suffers from an appreciably lower noise level, when compared to the other two solutions.

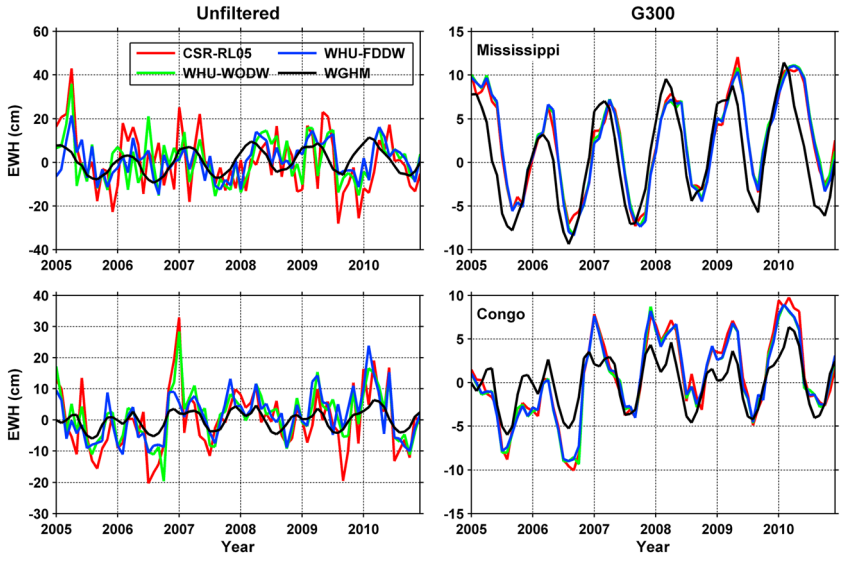

Figure 9. Time series of mean mass changes over the (top) Mississippi and (bottom) Congo river basins inferred from different GRACE solutions and the WGHM hydrological model.

Table 6
Annual Amplitudes (cm) and Phases (Day) of Mass Changes Over the Mississippi and Congo River Basins Derived From Different GRACE Solutions and the WGHM Hydrological Model

		Amplitude				Phase			
		WGHM	CSR-RL05	WHU-WODW	WHU-FDDW	WGHM	CSR-RL05	WHU-WODW	WHU-FDDW
Mississippi	Unfiltered	7.4	8.7	5.8	7.3	25.3	−27.2	−27.8	−25.6
	G150	-	7.1	6.6	7.1	-	−9.1	−8.7	−9.8
	G300	-	6.6	6.7	6.9	-	−2.3	−3.1	−3.6
Congo	Unfiltered	3.4	7.2	6.6	5.3	40.7	39.0	27.6	35.4
	G150	-	5.6	5.2	4.9	-	35.7	35.0	36.6
	G30	-	5.2	4.7	4.7	-	34.6	37.3	37.1

3.2. Analysis in the Spatial Domain

As the unfiltered solutions are corrupted by peculiar north-south stripes and high-frequency noise in the spatial domain, postprocessing is advised. In this study, we use the Gaussian filter (Wahr et al., 1998) to suppress the noise. To account for the impact of smoothing radius on the results, we consider two radii (150 and 300 km) and denote the solutions postprocessed in this way as the "G150 and G300 filtered solutions" hereafter. In addition, the C_{20} terms in all gravity field solutions are replaced by the SLR-derived values (Cheng et al., 2013). As regards the degree 1 terms which cannot be derived from GRACE-alone data, we use those determined by combining GRACE data and geophysical models as described in Sun et al. (2016, 2017).

To perform the analysis in the spatial domain, we first transform the monthly spherical harmonic coefficients to mass changes in terms of equivalent water heights on a $1° \times 1°$ grid as explained in Wahr et al. (1998). The correction for the Earth's oblateness has been applied as proposed by Ditmar (2018). As the Earth's surface mass changes (if exist) are primarily linear and seasonal, a deterministic model containing offset, trend, annual, and semiannual terms is fitted to the time series of gridded mass changes and regional mean mass changes. In this way, we obtain the trend and seasonal mass changes, as well as the residuals by subtracting the estimated dominant signal terms from the "observed" mass changes. This allows us to analyze the impacts of weighting scheme choice on the mass change signals and noise in the spatial domain.

To make the following discussion more comprehensive, we also quantify the level of random noise in the mass change time series using an independent approach. The approach is based on the regularization concept and assumes that (1) the target signal is close to a combination of an arbitrary annual periodic function and a long-term linear trend and (2) noise in the time series is white. According to this approach, the observed time series **d** is approximated with a regularized one **x** by minimizing the penalty function:

$$\phi(\mathbf{x}) = \frac{1}{\sigma_d^2}\sum_i(\mathbf{d}_i - \mathbf{x}_i)^2 + \frac{1}{\sigma_x^2}\Omega(\mathbf{x}) \tag{4}$$

where σ_d^2 is the noise variance, σ_x^2 is the signal variance, and $\Omega(\mathbf{x})$ is the regularization function which is designed such that periodic annual signals and a linear long-term trend in the data are not penalized. An estimation of the noise variance σ_d^2 and signal variance σ_x^2 is a part of the regularization procedure. For that

Table 7
Correlation Coefficients and RMS Mass Change Differences Between the GRACE Solutions and WGHM

		Correlation coefficients			RMS differences (cm)				
		CSR-RL05	WHU-WODW	WHU-FDDW	CSR-RL05	WHU-WODW	WHU-FDDW	$\frac{\text{FDDW}-\text{CSR}}{\text{CSR}}$	$\frac{\text{FDDW}-\text{WODW}}{\text{WODW}}$
Mississippi	Unfiltered	0.425	0.456	0.674	12.01	9.32	5.95	−50%	−36%
	G150	0.839	0.874	0.892	3.46	3.04	2.89	−16%	−5%
	G300	0.933	0.928	0.930	2.49	2.57	2.45	−2%	−5%
Congo	Unfiltered	0.592	0.652	0.676	8.49	7.54	6.00	−29%	−20%
	G150	0.802	0.811	0.828	3.79	3.44	3.15	−17%	−8%
	G300	0.839	0.840	0.846	2.93	2.71	2.63	−10%	−3%

Table 8
VCE-Based Noise Standard Deviations (cm) of the Mass Change Time Series Over the Mississippi and Congo River Basins Inferred From Different GRACE Solutions

		CSR-RL05	WHU-WODW	WHU-FDDW	$\frac{\text{FDDW}-\text{CSR}}{\text{CSR}}$	$\frac{\text{FDDW}-\text{WODW}}{\text{WODW}}$
Mississippi	Unfiltered	12.12	9.96	6.17	−49%	−38%
	G150	3.00	2.31	1.77	−41%	−23%
	G300	1.07	1.03	1.04	−3%	+1%
Congo	Unfiltered	8.11	6.42	4.82	−41%	−25%
	G150	2.37	2.41	2.06	−13%	−15%
	G300	1.16	1.17	1.10	−5%	−6%

purpose, the variance component estimation (VCE) technique (Koch & Kusche, 2002) is used. The resulting value of σ_d is used as an estimate of standard deviation (SD) of random noise in the considered data. For a more extended presentation of this approach, the reader is referred to Ditmar et al. (2018).

3.2.1. Gridded Mass Changes

Figure 6 displays geographical maps of the derived trends and periodic annual signals in mass changes from the unfiltered solutions. One can see that all the estimates indeed suffer from unrealistic stripes. It is hardly possible to identify regional signals, particularly at low to middle latitudes. A cross comparison of the three solutions under consideration reveals that the WHU-FDDW solution delivers the best recovery and shows the weakest stripes. As regards the G300 filtered solutions, we can see that the signal patterns recovered from different solutions are rather similar (Figure 7).

Figure 8 further displays the geographical distribution of the RMS residual mass changes. In the case of the unfiltered solutions, all RMS residuals present clear latitude-dependent behavior. This can be explained by the GRACE polar orbits, which lead to an increase in ground track density from the equator to the poles. In addition, ascending and descending ground tracks cross in polar areas at larger angles, which makes the sensitivity of GRACE observations more isotropic in this region. A comparison of different solutions shows that RMS residuals in the case of the WHU-FDDW solution are systematically smaller than those for the other two solutions. Assuming that the residual mass changes are dominated by noise, this indicates that the WHU-FDDW solution suffers from noise of a lower level than the others. Table 5 further lists the weighted mean of the RMS residual mass changes over the oceans and Sahara desert (the gridded RMS residuals are weighted by the cosine of latitude). Since temporal variations over oceans have been mostly removed by background models as described in Table 1, the residuals there are expected to contain more noise than over land areas, where residual signals can be noticeable (e.g., in the Amazon River Basin). One can see that RMS residuals over oceans in the case of the WHU-FDDW unfiltered solution are substantially reduced, when compared to the WHU-WODW and CSR-RL05 unfiltered solutions. And the results are well consistent with those obtained in the spectral domain (cf. Table 4). As far as the filtered solutions are concerned, the differences are substantially reduced with increasing smoothing radii, as can be observed from Table 5. This indicates that noise can be effectively suppressed with the Gaussian filter. As regards the Sahara desert, which is confined to the area (10°W–30°E, 20°N–30°N) in the computation, one should expect minimal temporal variations and thus noise-dominated residuals. It can be seen that the differences between RMS residuals

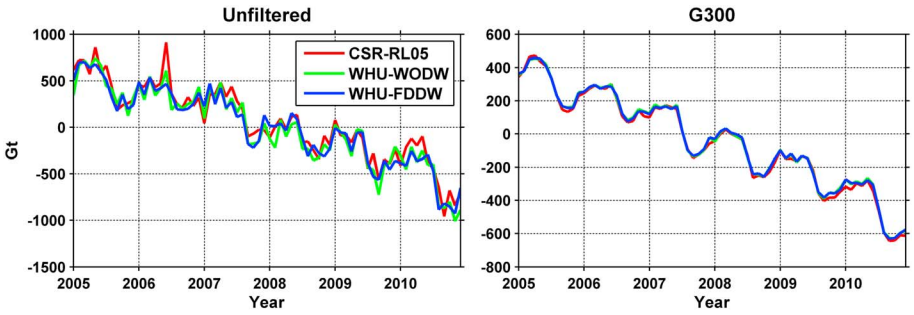

Figure 10. Time series of mean mass changes over Greenland inferred from different GRACE solutions.

Table 9
Mass Change Trends and Their Formal Errors (Gt/year) Over Greenland Inferred From Different GRACE Solutions

	CSR-RL05	WHU-WODW	WHU-FDDW
Unfiltered	−203±8.5	−211 ±9.6	−206 ± 7.0
G150	−178±3.9	−178 ± 4.2	−177 ± 3.5
G300	−152 ±2.6	−150 ± 2.6	−149 ± 2.5

for different solutions are not so significant when compared to those over the oceans. This may be partly attributed to leakage effects, which are likely similar in all three cases as can be seen in Figure 8.

3.2.2. Regional Mass Changes

To investigate the impacts of different weighting schemes on the recovery of mean regional signals, we select two large river basins (the Mississippi and Congo river basins), as well as Greenland as the target regions. Mass changes over the Mississippi river basin in North America have clear natural seasonality due to spring snowmelt in the mountainous areas and heavy rain in the plains during warm months (e.g., Rodell et al., 2006; Zaitchik et al., 2008). Mass changes over the Congo river basin in Africa also exhibit significant seasonal variations (Crowley et al., 2006). The river basin boundaries used in this study are taken from the website http://hydro.iis.u-tokyo.ac.jp/~taikan/TRIPDATA/TRIPDATA.html. As regards Greenland, it is known that the mass changes there show seasonal variations superimposed by a strong negative long-term trend (e.g., Ran et al., 2017; Schrama et al., 2014; Siemes et al., 2013; Velicogna & Wahr, 2013). The selected regions show different levels of errors in GRACE data as can be seen in Figure 8. Therefore, our selection of regions allows us to analyze the impacts of data weighting scheme for regions with both different error levels and different temporal behaviors of mass changes.

Figure 9 displays the time series of the mean mass changes over the Mississippi (top) and Congo (bottom) river basins derived from different solutions. In addition, we consider the time series derived from the WaterGAP Global Hydrology Model (denoted as "WGHM" hereafter), which is one of the most accurate global hydrological models at present (Döll, Müller Schmied, et al., 2014; Müller Schmied et al., 2016, 2014). It can be seen that the time series present different behaviors over the selected two river basins. In the case of Mississippi, GRACE time series exhibit similar amplitudes as WGHM but with phase lags of 1–2 months (cf. also Table 6). Over the Congo river basin, GRACE time series present clearly larger amplitudes, but with phase lags of only several days. Similar results were also reported by previous researches, but specific reasons for the differences between GRACE and WGHM still remain to be identified (Döll, Fritsche, et al., 2014; Schmidt et al., 2008). As regards differences between GRACE solutions, the WHU-FDDW solution shows a better consistency with WGHM in terms of annual amplitude in both unfiltered and filtered cases and over both river basins, as can be seen from Figure 9 and Table 6. We also compute the correlation coefficients of the mass change time series between the GRACE and WGHM solutions, as well as the RMS differences. To account for the phase discrepancies between GRACE and WGHM over Mississippi, the GRACE time series are shifted by one and two months for the filtered (G150 and G300) and unfiltered solutions, respectively. The results are listed in Table 7. One can see that the WHU-FDDW solution shows the strongest correlation with WGHM over both basins. The RMS differences between unfiltered WHU-FDDW solutions and WGHM over Mississippi are reduced substantially by 50 and 36%, respectively, when compared to the CSR-RL05 and WHU-WODW solutions. The reduction of RMS differences over Congo is also significant (29 and 20%, respectively). When looking into the filtered solutions, we see again improvements offered by the WHU-FDDW solutions though the improvements are smaller when compared to the unfiltered cases.

The VCE-based estimates of noise SD for different gravity field solutions are listed in Table 8. When considering the unfiltered solutions, the noise SD in the WHU-FDDW solutions is also substantially reduced when compared to the CSR-RL05 and WHU-WODW solutions. This agrees very well with the results obtained by the comparison between GRACE and WGHM (cf. Table 7). On the other hand, the differences between the estimates of noise SD for the filtered solutions become smaller with increasing smoothing radii (Table 7). Interestingly, the obtained estimates are clearly smaller than the RMS differences between the GRACE and WGHM time series. Most probably, this can be explained by the effect of filtering and the presence of inaccuracies in the WGHM time series. In principle, one may try to quantify those inaccuracies by combining the aforementioned RMS differences and the noise SD estimates (Ditmar, 2018). This is, however, beyond the scope of this research.

Table 10
VCE-Based Noise Standard Deviations (Gt) of the Mass Change Time Series Over Greenland Inferred From Different GRACE Solutions

	CSR-RL05	WHU-WODW	WHU-FDDW	$\frac{\text{FDDW}-\text{CSR}}{\text{CSR}}$	$\frac{\text{FDDW}-\text{WODW}}{\text{WODW}}$
Unfiltered	109	120	92	−16%	−23%
G150	39.9	35.5	30.7	−23%	−14%
G300	18.7	17.4	16.3	−13%	−6%

Figure 10 shows the time series of mass changes over Greenland. In all of the solutions, one can observe a strong negative trend due to a rapid ice mass loss there. As mentioned above, the time series is

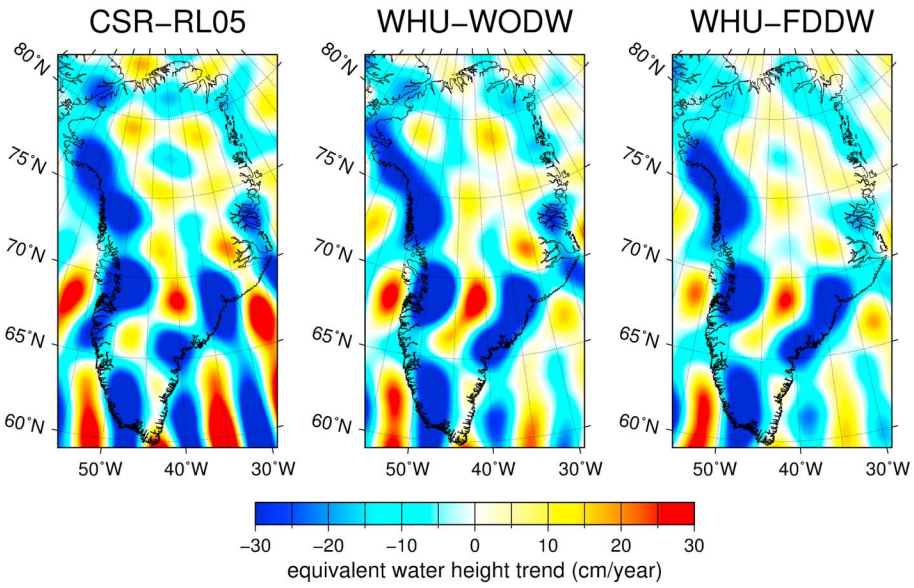

Figure 11. Trends in mass changes over Greenland inferred from different unfiltered GRACE solutions.

fitted by a deterministic model containing bias, trend, annual, and semiannual terms. We do not consider the acceleration of mass losses (Chen et al., 2006; Velicogna et al., 2014), since we cannot estimate it accurately due to the relatively short time period under consideration (Wouters et al., 2013). Table 9 lists the estimated trends, together with their formal errors, over Greenland. One can see that trend differences among different unfiltered solutions are not larger than 3%, whereas the formal errors in the case of the WHU-FDDW solution are substantially reduced by 18 and 27%, respectively, when compared to the CSR-RL05 and WHU-WODW solutions. When looking at the filtered solutions, we see that the trends in all three cases are very similar. All the values are significantly reduced, which is mainly caused by the smoothing effect of the filter. Table 10 shows the VCE-based estimates of noise SD for different mass change time series over Greenland. As can be seen, the noise reduction is significant in the case of the unfiltered WHU-FDDW solution (23%) and noticeable (14 and 6%) in the case of the two filtered WHU-FDDW solutions, when compared to the WHU-WODW solutions. As regards the comparison with CSR-RL05, the noise is reduced by 13 to 23%. The lower noise level over Greenland in the WHU-FDDW solution is also consistent with a higher accuracy of the estimated trend considered as a function of geographical coordinates, which can be clearly observed in Figure 11.

4. Conclusions

For the first time, we use the FDDW scheme to account for the colored noise in the context of the dynamic approach to the GRACE KRR data processing. In this way, we obtain improved estimates of monthly gravity field solutions. To demonstrate the added value of the FDDW scheme, we produce two sets of monthly gravity field solutions, one using the FDDW scheme ("WHU-FDDW" solutions) and the other one using the standard least squares adjustment ("WHU-WODW" solutions). In addition, the CSR RL05 solutions are considered. The solutions are compared in both spectral and spatial domains (in the latter case, both defined at grid nodes and averaged over selected regions). Comparison in the spectral domain as well as comparison of grids in the spatial domain show that the WHU-FDDW solutions suffer from noise of a lower level than the other two solutions. In the regional mass change recovery over the Mississippi and Congo river basins, the WHU-FDDW solution has shown a much better consistency with the state-of-the-art WaterGAP Global Hydrology Model than the others (the RMS differences with respect to WGHM are reduced at least by 29 and 20%, respectively, when compared to WHU-WODW and CSR-RL05). In addition, the VCE technique is applied to assess the standard deviation of random noise in the mass changes integrated over the two considered river basins and over Greenland. Again, the WHU-FDDW solutions clearly show the smallest noise levels among the three unfiltered solutions. When the filtered solutions are considered, however, the

differences between the solutions are substantially reduced (though the WHU-FDDW solutions still show a slightly higher performance in most cases). Thus, we conclude that the application of the FDDW scheme in the context of the dynamic approach may substantially reduce noise level in the resulting mass change estimates (particularly, if no filtering is applied).

We envision that the application of statistically optimal estimation techniques to data from the GRACE Follow-On (GFO) mission will be highly beneficial as well. Accelerometer noise as well as errors in models of ocean tides and nontidal mass variations in the atmosphere and ocean will likely be the factors limiting the GFO data accuracy (Flechtner et al., 2016). As a result, errors in those data will still be correlated. An enhanced estimation of gravity field using the FDDW scheme offers a way to alleviate the adverse impacts of these errors and, therefore, to improve the gravity field solutions.

Acknowledgments
The work was sponsored by the National "863 Program" of China (grant 2014AA121501) and the National Natural Science Foundation of China (grant 41574030). The numerical calculations in this research have been done on the supercomputing system in the Supercomputing Center of Wuhan University. The WaterGAP Global Hydrology Model (2.2c) used in this research is kindly provided by Hannes Müller Schmied and is available upon request. The GRACE level-1B data are publicly available from the ftp site: ftp://isdcftp.gfz-potsdam.de/grace/Level-1B. The CSR RL05 and WHU-FDDW (marked as "WHU RL01" and complete to degree and order 60/90/120) monthly solutions are publicly available from the International Center for Global Earth Model website: http://icgem.gfz-potsdam.de/series. The WHU-FDDW and WHU-WODW monthly solutions complete to degree and order 96 are available upon request. Finally, we thank the two anonymous reviewers for their helpful comments, which helped us improve the manuscript.

References

Bettadpur, S. (2012). GRACE UTCSR level-2 processing standards document for level-2 product release 0005 (17 pp.). Center for Space Research, University of Texas at Austin.

Bottoni, G. P., & Riccardo, B. (1993). Fast collocation. *Journal of Geodesy*, *67*(2), 119–126.

Chen, J. L., Wilson, C. R., & Seo, K. W. (2009). S2 tide aliasing in GRACE time-variable gravity solutions. *Journal of Geodesy*, *83*(7), 679–687. https://doi.org/10.1007/s00190-008-0282-1

Chen, J. L., Wilson, C. R., & Tapley, B. D. (2006). Satellite gravity measurements confirm accelerated melting of Greenland ice sheet. *Science*, *313*(5795), 1958–1960. https://doi.org/10.1126/science.1129007

Chen, Q., Shen, Y., Zhang, X., Hsu, H., & Chen, W. (2014). Global Earth's gravity field solution with GRACE orbit and range measurements using modified short arc approach. *Acta Geodaetica et Geophysica*, *50*(2), 173–185. https://doi.org/10.1007/s40328-014-0077-1

Chen, Q., Shen, Y., Zhang, X., Hsu, H., Chen, W., Ju, X., & Lou, L. (2015). Monthly gravity field models derived from GRACE level 1B data using a modified short-arc approach. *Journal of Geophysical Research: Solid Earth*, *120*, 1804–1819. https://doi.org/10.1002/2014jb011470

Cheng, M., & Ries, J. (2017). The unexpected signal in GRACE estimates of C_{20}. *Journal of Geodesy*, *91*(8), 897–914. https://doi.org/10.1007/s00190-016-0995-5

Cheng, M., Tapley, B. D., & Ries, J. C. (2013). Deceleration in the Earth's oblateness. *Journal of Geophysical Research: Solid Earth*, *118*, 740–747. https://doi.org/10.1002/jgrb.50058

Colombo, O. (1984). *The global mapping of gravity with two satellites*. Delft, Netherlands: Netherlands Geodetic Commission.

Crowley, J. W., Mitrovica, J. X., Bailey, R. C., Tamisiea, M. E., & Davis, J. L. (2006). Land water storage within the Congo Basin inferred from GRACE satellite gravity data. *Geophysical Research Letters*, *33*, L19402. https://doi.org/10.1029/2006GL027070

Dahle, C., Flechtner, F., Gruber, C., König, D., König, R., Michalak, G., & Neumayer, K. H. (2012). GFZ GRACE level-2 processing standards document for level-2 product release 0005, (Scientific Technical Report STR 12/02 – Data, Revised Edition, January 2013), Potsdam (21 pp.). https://doi.org/10.2312/GFZ.b103-1202-25

Desai, S. D. (2002). Observing the pole tide with satellite altimetry. *Journal of Geophysical Research*, *107*(C11), 3186. https://doi.org/10.1029/2001JC001224

Ditmar, P. (2018). Conversion of time-varying stokes coefficients into mass anomalies at the Earth's surface considering the Earth's oblateness. *Journal of Geodesy*. https://doi.org/10.1007/s00190-018-1128-0

Ditmar, P., Klees, R., & Liu, X. (2007). Frequency-dependent data weighting in global gravity field modeling from satellite data contaminated by non-stationary noise. *Journal of Geodesy*, *81*(1), 81–96. https://doi.org/10.1007/s00190-006-0074-4

Ditmar, P., Kuznetsov, V., Van Eck van der Sluijs, A. A., Schrama, E. J. O., & Klees, R. (2006). 'DEOS_CHAMP-01C_70': A model of the Earth's gravity field computed from accelerations of the CHAMP satellite. *Journal of Geodesy*, *79*(10-11), 586–601. https://doi.org/10.1007/s00190-005-0008-6

Ditmar, P., Tangdamrongsub, N., Ran, J., & Klees, R. (2018). Estimation and reduction of random noise in mass anomaly time-series from satellite gravity data by minimization of month-to-month year-to-year double differences. *Journal of Geodynamics*, *119*, 9–22. https://doi.org/10.1016/j.jog.2018.05.003

Ditmar, P., Teixeira da Encarnação, J., & Hashemi Farahani, H. (2012). Understanding data noise in gravity field recovery on the basis of inter-satellite ranging measurements acquired by the satellite gravimetry mission GRACE. *Journal of Geodesy*, *86*(6), 441–465. https://doi.org/10.1007/s00190-011-0531-6

Dobslaw, H., Bergmann-Wolf, I., Forootan, E., Dahle, C., Mayer-Gürr, T., Kusche, J., & Flechtner, F. (2016). Modeling of present-day atmosphere and ocean non-tidal de-aliasing errors for future gravity mission simulations. *Journal of Geodesy*, *90*(5), 423–436. https://doi.org/10.1007/s00190-015-0884-3

Döll, P., Fritsche, M., Eicker, A., & Müller Schmied, H. (2014). Seasonal water storage variations as impacted by water abstractions: Comparing the output of a global hydrological model with GRACE and GPS observations. *Surveys in Geophysics*, *35*(6), 1311–1331. https://doi.org/10.1007/s10712-014-9282-2

Döll, P., Müller Schmied, H., Schuh, C., Portmann, F. T., & Eicker, A. (2014). Global-scale assessment of groundwater depletion and related groundwater abstractions: Combining hydrological modeling with information from well observations and GRACE satellites. *Water Resources Research*, *50*(7), 5698–5720. https://doi.org/10.1002/2014WR015595

Farahani, H. H., Ditmar, P., Inácio, P., Didova, O., Gunter, B., Klees, R., et al. (2017). A high resolution model of linear trend in mass variations from DMT-2: Added value of accounting for coloured noise in GRACE data. *Journal of Geodynamics*, *103*, 12–25. https://doi.org/10.1016/j.jog.2016.10.005

Farahani, H. H., Ditmar, P., & Klees, R. (2014). Assessment of the added value of data from the GOCE satellite mission to time-varying gravity field modelling. *Journal of Geodesy*, *88*(2), 157–178. https://doi.org/10.1007/s00190-013-0674-8

Flechtner, F., Dobslaw, H., & Fagiolini, E. (2015). AOD1B Product Description Document for Product Release 05, Edited, GFZ German Research Centre for Geosciences.

Flechtner, F., Neumayer, K.-H., Dahle, C., Dobslaw, H., Fagiolini, E., Raimondo, J.-C., & Güntner, A. (2016). What can be expected from the GRACE-FO laser ranging interferometer for earth science applications? *Surveys in Geophysics*, *37*(2), 453–470. https://doi.org/10.1007/s10712-015-9338-y

Folkner, W. M., Williams, J. G., & Boggs, D. H. (2009). The Planetary and Lunar Ephemeris DE 421 (pp. 1–34). Jet Propulsion Laboratory, California Institute of Technology.
Förste, C., Bruinsma, S. L., Abrikosov, O., Lemoine, J.-M., Marty, J. C., Flechtner, F., et al. (2014). EIGEN-6C4 the latest combined global gravity field model including GOCE data up to degree and order 2190 of GFZ Potsdam and GRGS Toulouse, GFZ Data Services. http://doi.org/10.5880/icgem.2015.1
Guo, X., & Zhao, Q. (2018). GRACE time-varying gravity field solutions based on PANDA software. *Geodesy and Geodynamics*, *9*(2), 162–168. https://doi.org/10.1016/j.geog.2017.11.003
Inácio, P., Ditmar, P., Klees, R., & Farahani, H. H. (2015). Analysis of star camera errors in GRACE data and their impact on monthly gravity field models. *Journal of Geodesy*, *89*(6), 551–571. https://doi.org/10.1007/s00190-015-0797-1
Jäggi, A., Hugentobler, U., Bock, H., & Beutler, G. (2007). Precise orbit determination for GRACE using undifferenced or doubly differenced GPS data. *Advances in Space Research*, *39*(10), 1612–1619. https://doi.org/10.1016/j.asr.2007.03.012
Kang, Z., Tapley, B., Bettadpur, S., Ries, J., Nagel, P., & Pastor, R. (2006). Precise orbit determination for the GRACE mission using only GPS data. *Journal of Geodesy*, *80*(6), 322–331. https://doi.org/10.1007/s00190-006-0073-5
Kim, J. (2000). *Simulation study of a low-low satellite-to-satellite tracking mission*, (PhD thesis). The University of Texas at Austin.
Klees, R., Ditmar, P., & Broersen, P. (2003). How to handle colored observation noise in large least-squares problems. *Journal of Geodesy*, *76*(11–12), 629–640. https://doi.org/10.1007/s00190-002-0291-4
Klinger, B., & Mayer-Gürr, T. (2016). The role of accelerometer data calibration within GRACE gravity field recovery: Results from ITSG-Grace2016. *Advances in Space Research*, *58*(9), 1597–1609. https://doi.org/10.1016/j.asr.2016.08.007
Koch, K. R., & Kusche, J. (2002). Regularization of geopotential determination from satellite data by variance components. *Journal of Geodesy*, *76*(5), 259–268. https://doi.org/10.1007/s00190-002-0245-x
Liu, J., & Ge, M. (2003). PANDA software and its preliminary result of positioning and orbit determination. *Wuhan University Journal of Natural Sciences*, *8*(2), 603–609.
Liu, X., Ditmar, P., Siemes, C., Slobbe, D. C., Revtova, E., Klees, R., et al. (2010). DEOS mass transport model (DMT-1) based on GRACE satellite data: Methodology and validation. *Geophysical Journal International*, *181*(2), 769–788. https://doi.org/10.1111/j.1365-246X.2010.04533.x
McCullough, C., & Bettadpur, S. (2016). *Improvements in GRACE gravity field determination through stochastic observation modeling*. Paper Presented at AGU Fall Meeting Abstracts.
Meyer, U., Jäggi, A., Jean, Y., & Beutler, G. (2016). AIUB-RL02: An improved time-series of monthly gravity fields from GRACE data. *Geophysical Journal International*, *205*(2), 1196–1207. https://doi.org/10.1093/gji/ggw081
Müller Schmied, H., Adam, L., Eisner, S., Fink, G., Flörke, M., Kim, H., et al. (2016). Variations of global and continental water balance components as impacted by climate forcing uncertainty and human water use. *Hydrology and Earth System Sciences*, *20*(7), 2877–2898. https://doi.org/10.5194/hess-20-2877-2016
Müller Schmied, H., Eisner, S., Franz, D., Wattenbach, M., Portmann, F. T., Flörke, M., & Döll, P. (2014). Sensitivity of simulated global-scale freshwater fluxes and storages to input data, hydrological model structure, human water use and calibration. *Hydrology and Earth System Sciences*, *18*(9), 3511–3538. https://doi.org/10.5194/hess-18-3511-2014
Pail, R., Gruber, T., & Fecher, T. (2016). The combined gravity model GOCO05c. GFZ data services. https://doi.org/10.5880/icgem.2016.003
Petit, G., & Luzum, B. (2010). *IERS Conventions (2010), edited, Verlag des Bundesamts für Kartographie und Geodäsie*. Germany: Frankfurt am Main.
Ran, J., Ditmar, P., Klees, R., & Farahani, H. H. (2017). Statistically optimal estimation of Greenland ice sheet mass variations from GRACE monthly solutions using an improved mascon approach. *Journal of Geodesy*, *92*(3), 299–319. https://doi.org/10.1007/s00190-017-1063-5
Ray, R. D., & Luthcke, S. B. (2006). Tide model errors and GRACE gravimetry: Towards a more realistic assessment. *Geophysical Journal International*, *167*(3), 1055–1059. https://doi.org/10.1111/j.1365-246X.2006.03229.x
Rieser, D., Mayer-Gürr, T., Savcenko, R., Bosch, W., Wünsch, J., Dahle, C., & Flechtner, F. (2012). The Ocean Tide Model EOT11a in Spherical Harmonics Representation, Institute of Theoretical Geodesy and Satellite Geodesy (ITSG), TU Graz, Austria; Deutsches Geodätisches Forschungsinstitut (DGFI), Munich, Germany; GFZ German Research Centre for Geosciences, Potsdam, Germany.
Rodell, M., Chen, J., Kato, H., Famiglietti, J. S., Nigro, J., & Wilson, C. R. (2006). Estimating groundwater storage changes in the Mississippi River basin (USA) using GRACE. *Hydrogeology Journal*, *15*(1), 159–166. https://doi.org/10.1007/s10040-006-0103-7
Schmidt, R., Petrovic, S., Güntner, A., Barthelmes, F., Wünsch, J., & Kusche, J. (2008). Periodic components of water storage changes from GRACE and global hydrology models. *Journal of Geophysical Research*, *113*, B08419. https://doi.org/10.1029/2007JB005363
Schrama, E. J. O., Wouters, B., & Rietbroek, R. (2014). A mascon approach to assess ice sheet and glacier mass balances and their uncertainties from GRACE data. *Journal of Geophysical Research: Solid Earth*, *119*, 6048–6066. https://doi.org/10.1002/2013jb010923
Seo, K. W., Wilson, C. R., Han, S. C., & Waliser, D. E. (2008). Gravity Recovery And Climate Experiment (GRACE) alias error from ocean tides. *Journal of Geophysical Research*, *113*, B03405. https://doi.org/10.1029/2006JB004747
Shi, C., Zhao, Q., Geng, J., Lou, Y., Ge, M., & Liu, J. (2008). *Recent Development of PANDA Software in GNSS Data Processing*. Paper Presented at Proceedings of the Society of Photographic Instrumentation Engineers.
Siemes, C., Ditmar, P., Riva, R. E. M., Slobbe, D. C., Liu, X. L., & Farahani, H. H. (2013). Estimation of mass change trends in the Earth's system on the basis of GRACE satellite data, with application to Greenland. *Journal of Geodesy*, *87*(1), 69–87. https://doi.org/10.1007/s00190-012-0580-5
Sun, Y., Ditmar, P., & Riva, R. (2017). Statistically optimal estimation of degree-1 and C20 coefficients based on GRACE data and an ocean bottom pressure model. *Geophysical Journal International*, *210*(3), 1305–1322. https://doi.org/10.1093/gji/ggx241
Sun, Y., Riva, R., & Ditmar, P. (2016). Optimizing estimates of annual variations and trends in geocenter motion and J_2 from a combination of GRACE data and geophysical models. *Journal of Geophysical Research: Solid Earth*, *121*, 8352–8370. https://doi.org/10.1002/2016jb013073
Tapley, B. D., Bettadpur, S., Ries, J. C., Thompson, P. F., & Watkins, M. M. (2004). GRACE measurements of mass variability in the earth system. *Science*, *305*(5683), 503–505. https://doi.org/10.1126/science.1099192
Velicogna, I., Sutterley, T. C., & van den Broeke, M. R. (2014). Regional acceleration in ice mass loss from Greenland and Antarctica using GRACE time-variable gravity data. *Geophysical Research Letters*, *41*(22), 8130–8137. https://doi.org/10.1002/2014gl061052
Velicogna, I., & Wahr, J. (2013). Time-variable gravity observations of ice sheet mass balance: Precision and limitations of the GRACE satellite data. *Geophysical Research Letters*, *40*, 3055–3063. https://doi.org/10.1002/grl.50527
Visser, P. N. A. M., Sneeuw, N., Reubelt, T., Losch, M., & van Dam, T. (2010). Space-borne gravimetric satellite constellations and ocean tides: Aliasing effects. *Geophysical Journal International*. https://doi.org/10.1111/j.1365-246X.2010.04557.x
Wahr, J., Molenaar, M., & Bryan, F. (1998). Time variability of the Earth's gravity field: Hydrological and oceanic effects and their possible detection using GRACE. *Journal of Geophysical Research*, *103*(B12), 30,205–30,229. https://doi.org/10.1029/98JB02844
Watkins, M. M., & Yuan, D. N. (2014). GRACE JPL level-2 processing standards document for level-2 product release 05.1 (14 pp.). Jet Propulsion Laboratory, California Institute of Technology.

Wouters, B., Bamber, J. L., van den Broeke, M. R., Lenaerts, J. T. M., & Sasgen, I. (2013). Limits in detecting acceleration of ice sheet mass loss due to climate variability. *Nature Geoscience*, *6*(8), 613–616. https://doi.org/10.1038/ngeo1874

Wu, S. C., Kruizinga, G., & Bertiger, W. (2006). Algorithm theoretical basis document for GRACE level-1B data processing v1.2. Jet Propulsion Laboratory, California Institute of Technology.

Zaitchik, B. F., Rodell, M., & Reichle, R. H. (2008). Assimilation of GRACE terrestrial water storage data into a land surface model: Results for the Mississippi River basin. *Journal of Hydrometeorology*, *9*(3), 535–548. https://doi.org/10.1175/2007jhm951.1

Zhao, Q., Guo, J., Hu, Z., Shi, C., Liu, J., Cai, H., & Liu, X. (2011). GRACE gravity field modeling with an investigation on correlation between nuisance parameters and gravity field coefficients. *Advances in Space Research*, *47*(10), 1833–1850. https://doi.org/10.1016/j.asr.2010.11.041